ISIJ International, Vol. 34 (1994), No. 4, pp. 359–365

Precipitation Hardening in Fe–Cu Binary and Quaternary Alloys

Kozo OSAMURA, Hiroshi OKUDA, Shojiro OCHIAI, Minoru TAKASHIMA, Kazuo ASANO, Michihiro FURUSAKA,[1] Koji KISHIDA[2] and Fumio KUROSAWA[3]

Mesoscopic Materials Research Center, Faculty of Engineering, Kyoto University, Yoshida-honmachi, Sakyo-ku, Kyoto, Kyoto-fu, 606 Japan. 1) National Laboratory for High Energy Physics, Oho, Tsukuba, Ibaraki-ken, 305 Japan. 2) Hirohata R & D Laboratories, Nippon Steel Corporation, Fuji-cho, Hirohata-ku, Himeji, Hyogo-ken, 671-11 Japan. 3) Advanced Materials and Technology Research Laboratories, Nippon Steel Corporation, Shintomi, Futtsu, Chiba-ken, 299-12 Japan.

(*Received on August 27, 1993; accepted in final form on December 17, 1993*)

The behavior of precipitation hardening in two types of Fe–Cu alloys has been investigated by means of mechanical tests as well as small angle neutron scattering measurements. The integrated intensity increased first and reached a constant corresponding to the completion of precipitation reaction, while particle radius increased monotonically with aging time, where Vickers hardness and yield stress increased and reached maxima, then decreased. The interaction force with a dislocation due to each precipitate was very small compared with the force by the Orowan mechanism. After discussion based on three possible mechanisms in terms of coherency strain, elastic modulus change and interfacial energy, the strengthening was suggested to be caused from the coherency strain effect. The first increase of yield stress during aging is attributed to the growth in size of clusters and the decrease of yield stress after the maximum is mainly related to the decrease of number density of precipitates. It was found that the loss of coherency with the matrix greatly lowers the strengthening effect, whereby the structure of precipitates changes from bcc to fcc during aging.

KEY WORDS: yield stress; Vickers hardness; small-angle neutron scattering; Fe–Cu alloy; copper-rich cluster; precipitation hardening; coherency strain.

1. Introduction

Since the precipitation phenomenon in the Fe–Cu alloy was first reported in 1958,[1] the details of structural change as well as mechanical properties have been investigated by many authors.[2–8] It has been made clear that bcc metastable copper-rich clusters first precipitate from supersaturated α iron and then transform to ε-Cu(fcc) phase when they grow beyond a critical size. Copper-rich precipitates are spherical at the early stage, but their shape changes to rod or ellipsoid due to the strain energy term. The interrelation between hardness and microstructure have been investigated[2,4] and the mechanism of precipitation hardening was discussed.[5,9] As pointed out by Russel and Brown,[5] the high work-hardening rates expected at the overaging condition were not observed in the present iron–copper system. They proposed a theory based on an interaction between matrix slip dislocations and obstacles with lower elastic modulus than the matrix materials, which was able to account for both the observed yield strength and the work hardening behavior. However the relation of their theory with respect to internal structure of precipitates and its change during aging was not explained.

From a practical viewpoint, copper-rich precipitates were reported to induce embrittlement in the pressure vessel for the atomic reactor.[6] On the other hand, the age-hardenable copper bearing steel has been developed as a high strength steel with excellent performance for low-temperature toughness and hydrogen induced cracking resistance.[10,11]

Since the mechanism of precipitation hardening is not yet clearly understood, especially in the microstructural aspect, a more quantitative information on the interaction between dislocation and precipitates is essential for designing high performance steel. In our previous papers,[8,12] the structure of precipitated alloy and its change during aging were investigated in Fe–Cu binary alloy and the effect of nickel and manganese addition on the microstructure evolution was determined. Here, in order to elucidate the mechanism of precipitation hardening in the present Fe–Cu alloy systems, mechanical tests and small-angle neutron scattering (SANS) measurements were carried out. With the aid of structural parameters determined here, the interaction of dislocation with precipitates was analysed in detail.

2. Experimental Procedure

Two types of Fe–Cu alloys were used in the present study; their chemical composition is listed in **Table 1**. Hereafter these alloys are referred to as binary and quaternary, respectively. After forging and hot-rolling, small pieces with dimensions of $2.7 \times 10 \times 100$ and

Table 1. Chemical composition in at% of Fe–Cu alloys used here.

Sample name	C	Si	Mn	P	S	Cu	Ni	Al	Ti	N	B	O
Binary	0.019	0.002	0.01	—	0.014	1.17	—	0.015	—	0.005	—	0.01
Quaternary	0.0061	0.024	0.25	0.031	0.007	1.41	0.27	0.114	0.053	0.0052	0.0021	—

$2.7 \times 10 \times 30\,mm^3$ were prepared for tensile test and SANS measurements, respectively. After the specimen was solution-treated at 1 123 K for 10.8 ks in the α primary phase region, it was quenched into ice water. Specimen were isothermally aged at 773 and 823 K.

The tensile test was carried out using the Instron-type testing machine; 0.2% proof stress and tensile strength were measured. In this paper 0.2% proof stress is regarded as yield stress. Vickers hardness was measured on the polished surface after aging.

SANS measurements were performed using the KENS-SAN facilities of National Laboratory for High Energy Physics, KEK. The details have been reported elsewhere.[8] Scattering intensities were measured by a two-dimensional position sensitive detector in the scattering vector ($|Q|=4\pi\sin\theta/\lambda$) range from 0.06 to $3\,nm^{-1}$. In general, the scattering intensity is composed of both magnetic and nuclear components for a ferromagnetic material. To separate the two contributions, the external magnetic field of about one tesla was applied in the horizontal direction perpendicular to the incident neutron beam. The SANS measurements were carried out at room temperature and using the same specimen, Vickers hardness was measured.

3. Experimental Results

Figure 1 shows the change of Vickers hardness as a function of aging time for the specimens aged at 773 and 823 K. Peak hardness appears earlier, when the specimen was aged at the higher temperature. When aged at the same temperature, peak hardness became higher for the quaternary alloy. As reported by several investigators,[2,4,5,9,13] the time reaching peak hardness was found to be between 7 and 20 ks for specimens containing 0.79 to 1.48 at% Cu, when aged at 773 K.

Figure 2 shows the change of yield stress as a function of aging time for the specimens aged at 773 and 823 K. Their behavior is very similar to the change of hardness. The relation between Vickers hardness in units of kg/mm^2 and yield stress in units of MPa was examined by comparing the experimental data in Figs. 1 and 2. The correlation between them is clearly seen in **Fig. 3** as expressed in average by the equation, $\sigma_y=2.7H_v-140$. The reported data[5] are also plotted in this figure for comparison, where the ferrite grain sizes were reported to be 40 μm. Using this relation, the yield stress is hereafter estimated from Vickers hardness for the present discussion.

SANS intensity provides structural information on precipitates as described previously in detail.[8,12] The neutron scattering intensity consists of both magnetic and nuclear components for the ferromagnetic specimen containing paramagnetic particles. By applying a strong magnetic field to the specimen, it is possible to separate these two components. The magnetic scattering component is suggested to be directly related to paramagnetic particles, namely, copper-rich clusters.[12] The scattering intensity has been analysed by assuming the precipitated structure in which Cu-rich spherical clusters per unit volume distribute randomly in the matrix with number density of N_p. Then the magnetic scattering intensity $(d\Sigma/d\Omega)_{MAG}$ is given by the equation;

$$\left(\frac{d\Sigma}{d\Omega}\right)_{MAG}=(\Delta\rho)^2_{MAG}N_p\int F(R)\left(\frac{4}{3}\pi R^3\right)^2|\Phi(RQ)|^2\,dR\,, \quad \text{.....(1)}$$

where $\Delta\rho_{MAG}$ is the difference in the magnetic scattering length density between matrix and cluster, $F(R)$ is the

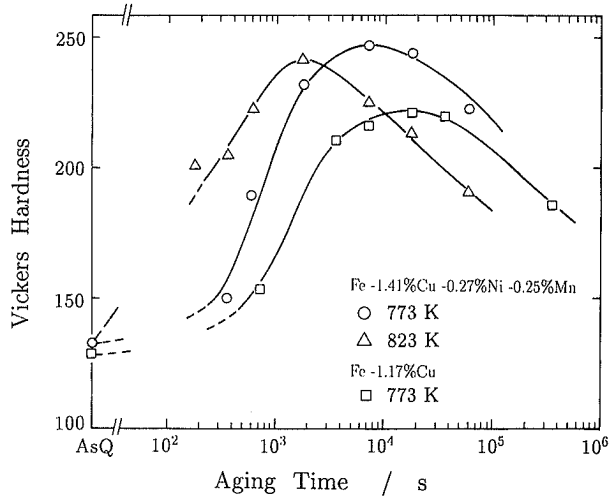

Fig. 1. Change of Vickers hardness as a function of aging time for Fe–Cu binary and quaternary alloys aged at 773 and 823 K.

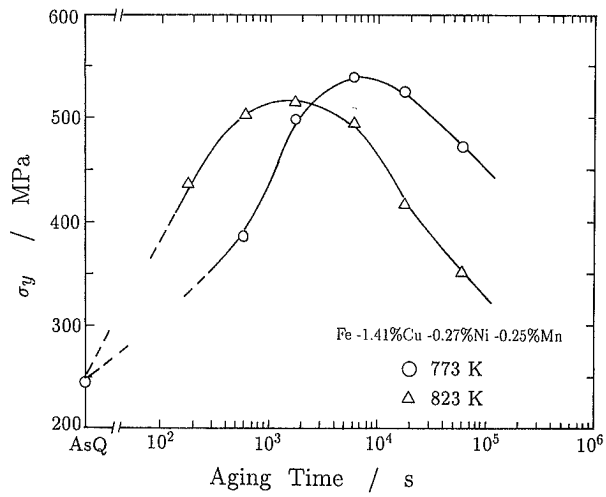

Fig. 2. Change of yield stress as a function of aging time for Fe–Cu quaternary alloys aged at 773 and 823 K.

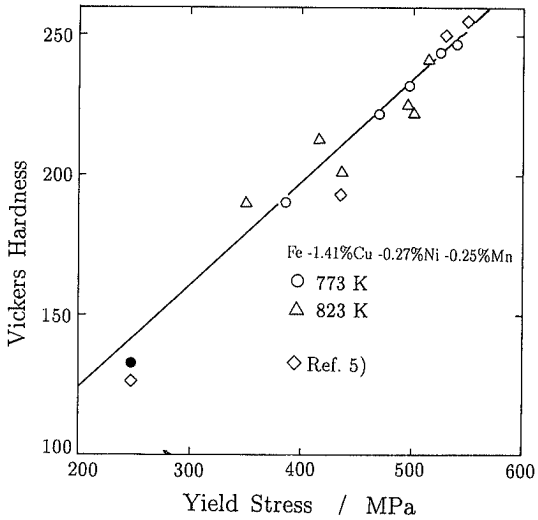

Fig. 3. Correlation between Vickers hardness and yield stress for Fe–Cu quaternary alloys aged at 773 and 823 K where the closed circle is the value for the as-quenched state.

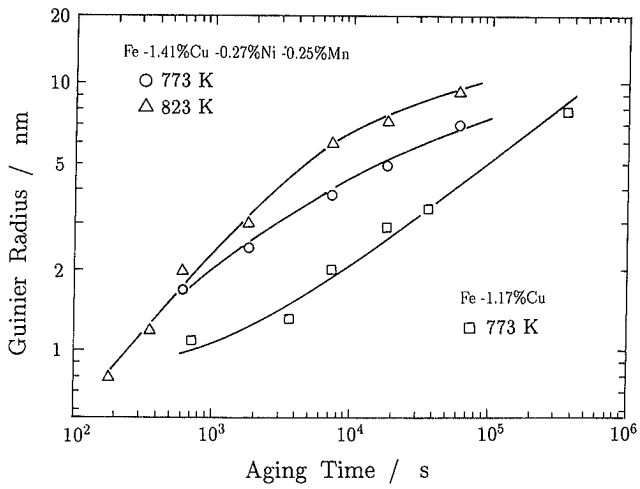

Fig. 4. Aging time dependence of Guinier radius for Fe–Cu binary and quaternary alloys aged at 773 and 823 K.

size distribution function, R is the cluster radius and $\Phi(QR)$ is the form factor for a cluster.

Guinier radius can be obtained from the Q-dependence of SANS intensity, which is an average value of cluster radii. **Figure 4** shows the aging time dependence of Guinier radius. In the quaternary alloy, the radius increases with aging time and tends to saturate at longer aging time. For the binary alloy, on the other hand, the aging time dependence differs. The radius tends to increase, being proportional to $(\text{time})^{1/3}$, when the specimen was aged for a time longer than 3.6 ks. Another kind of radius, Porod radius (R_p) is important for discussing the size distribution of precipitates. The statistical meaning of the Porod radius was explained in our previous paper[12] and can be experimentally deduced from the Fourier transform of SANS intensity. The result of R_p for the specimen mentioned above was already reported previously.[12]

Figure 5 shows the integrated intensity (Z_o) for the quaternary specimens aged isothermally. It is proportional to the volume fraction (V_f) of precipitates, when

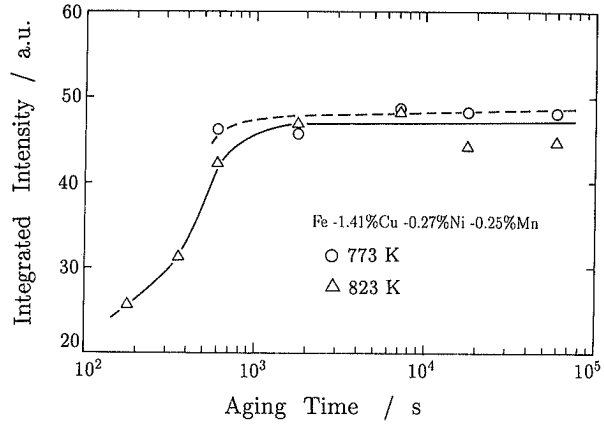

Fig. 5. Aging time dependence of the integrated intensity for Fe–Cu quaternary alloys aged at 773 and 823 K.

$\Delta\rho_{MAG}$ remains constant. After rapidly increasing in a short aging period, the integrated intensity became constant (Z_o^∞), indicating that the precipitation reaction had been completed. When this saturated volume fraction is expressed as V_f^∞, it is approximately given by the equation:

$$V_f^\infty = \frac{x_{Cu,o} - x_{Cu,m}}{x_{Cu,p} - x_{Cu,m}}, \quad \text{.....(2)}$$

where $x_{Cu,o}$ is mole fraction of Cu component in the alloy, and $x_{Cu,p}$ and $x_{Cu,m}$ are the value in the precipitate and the matrix, respectively. Then, the volume fraction at any time is given by $V_f = V_f^\infty (Z_o/Z_o^\infty)$.

The size distribution function ($F(R)$) for precipitates has been assumed to obey a log-normal size distribution as discussed previously,[8] which is given by the equation:

$$F(R) = \frac{1}{\sqrt{2\pi}R\ln\sigma}\exp\left[-\frac{1}{2}\left(\frac{\ln R - \ln\mu}{\ln\sigma}\right)^2\right], \quad \text{....(3)}$$

where μ and σ are the mean radius and the standard deviation, respectively. These two size parameters are estimated from the experimentally determined Guinier (R_G) and Porod (R_P) radii by using the following equations:

$$\mu = \exp\left[\ln R_G - \frac{14}{9}\ln\left(\frac{R_G}{R_P}\right)\right], \quad \text{.....(4)}$$

$$\sigma = \exp\left\{\left[\frac{2}{9}\ln\left(\frac{R_G}{R_P}\right)\right]^{1/2}\right\}. \quad \text{.....(5)}$$

Using these two relations, the mean radius and the standard deviation have been numerically evaluated as shown in **Fig. 6**. The radius increased with increasing aging time, while the standard deviation remained constant over the whole aging time. As mentioned in the previous report,[8] nevertheless clusters have either bcc or fcc crystal structure, they obey the same size distribution.

As an average structure, the volume fraction is expressed as a function of mean radius and number density of precipitates as

$$V_f = \frac{4}{3}\pi\mu^3 N_p, \quad \text{.....(6)}$$

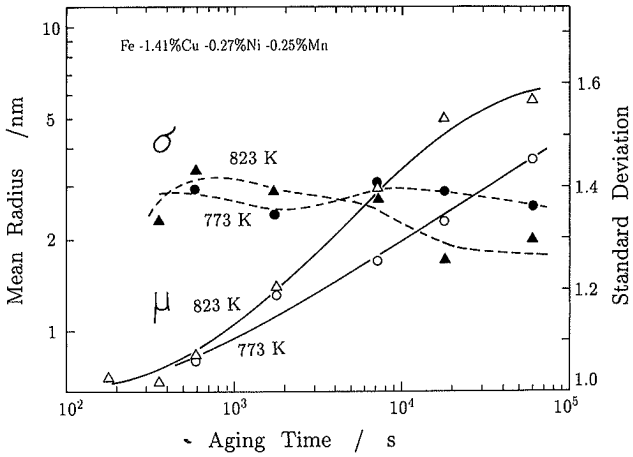

Fig. 6. Change of mean radius (μ) and standard deviation (σ) as a function of aging time for Fe–Cu quaternary alloys aged at 773 and 823 K, where the log-normal size distribution is assumed.

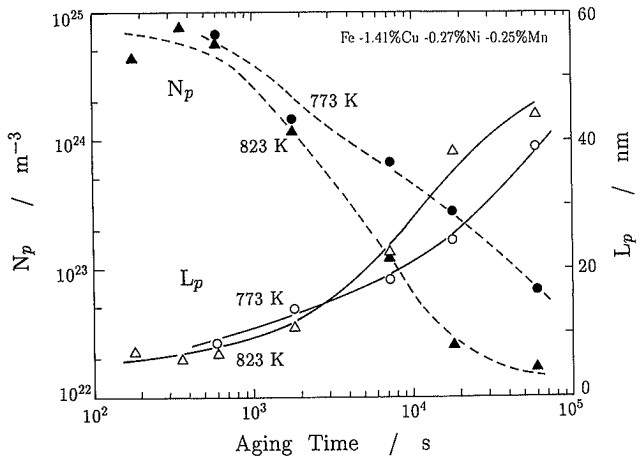

Fig. 7. Change of three dimensional interparticle distance (L_p) and number density (N_p) of precipitates as a function of aging time for Fe–Cu quaternary alloys aged at 773 and 823 K.

where the number density N_p is given by the equation:

$$N_p = \frac{\kappa}{L_p^3}, \quad \text{.....(7)}$$

where κ is $\sqrt{2}$, when precipitates are closely packed with interparticle distance L_p. **Figure 7** shows the change of L_p and N_p as a function of aging time. In the short aging period, the number density was high, but decreased rapidly during aging. The interparticle distance became larger with increasing aging time, indicating that the coarsening process takes place, while the standard deviation remained constant as shown in Fig. 6.

4. Discussion

Knowledge on the precipitated structure of the present alloy systems is summarized in the following. Several attempts have been made in order to determine the chemical composition in clusters of nm size. Worrel *et al.*[13] found by field ion microscope-atom probe (FIM-AP) analysis that the precipitates in the over-aged specimens contain less than a few % iron. The SANS

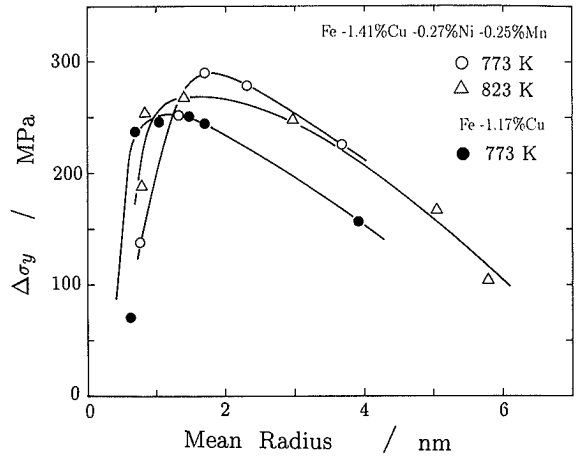

Fig. 8. Change of yield stress as a function of mean particle radius for Fe–Cu quaternary alloys aged at 773 and 823 K.

data of Kampmann and Wagner[14] suggested that all precipitates larger than 1 nm are pure copper. As reported,[8] the chemical composition of the precipitates was pure copper in the Fe–Cu binary alloy. In the quaternary alloy, the segregated layer enriched by Ni and Mn was found to be formed around fcc copper-rich precipitates by means of FIM-AP and SANS techniques.[12]

Homogeneous nucleation of bcc clusters occurs preferentially in the matrix as suggested by Hornbogen.[3] These bcc clusters grow in size and transform to fcc ε precipitates beyond a critical size, at which loss of coherency occurs. The critical radius was reported to be 1.6 nm from the classical nucleation theory,[12] and to be about 4.5[2] and 2.5 nm[15] experimentally. Precipitates are spherical at the early stage, but their shape changes to rod[3] or ellipsoid[12] due to strain energy term, when their particle radius exceeds about 15 nm.[3]

Figure 8 shows the relation between yield stress and mean radius, where $\Delta\sigma_y = \sigma - \sigma_{As\text{-}Q}$, and $\sigma_{As\text{-}Q}$ is the yield stress for the as-quenched specimen. The maximum yield stress appears at 1.2–1.7 nm. The change of yield stress might have a complex structure dependence, because it is a function of particle size, interparticle distance, change of internal structure and so on. Youle and Ralph[16] observed peak hardness at 21.6 ks for the Fe–1.5at%Cu alloy aged at 743 K, where they estimated an average radius of 1.8 nm. Also, Goodman *et al.*[15] reported that the mean radius at maximum strength is about 1.2 nm. Buswell *et al.*[6] found the mean radius of 2 nm for peak hardness when the Fe–1.14at%Cu alloy was aged at 823 K. The present experimental data are therefore found to be in reasonably good agreement with those reported.

In order to understand the microstructure dependence of yield stress, the mechanism of interaction between dislocation and precipitate will be discussed in the following. The important thing is that the present structure analysis showed an average structure consisting of many particles with size distribution and the mechanism will be discussed on statistics.

4.1. Interaction Force with a Dislocation due to an Obstacle

When a glide dislocation encounters an array of obstacles, it bows out with a curvature between two obstacles. According to Brown and Ham's analysis[17] based on Foreman and Makin's numerical solution, the critical shear stress at which a dislocation can move a large distance through an array of obstacles is a function of the obstacle spacing (L) on the slip plane and the critical angle (ϕ_c). The shear stress is given by

$$\tau=\frac{1.6T}{bL}\cos\left(\frac{\phi_c}{2}\right), \quad \phi_c<100^\circ, \quad \text{.....(10a)}$$

$$\tau=\frac{2T}{bL}\left[\cos\left(\frac{\phi_c}{2}\right)\right]^{3/2}, \quad \phi_c>100^\circ, \quad \text{....(10b)}$$

where T is the line tension and b Burgers vector. When the three dimensional interparticle distance among obstacles is given by L_p as defined from center to center, the two dimensional obstacle spacing (L) on the slip plane is given as

$$L=\left(\frac{\pi}{12V_f}\right)^{1/6}L_p-2\sqrt{\frac{2}{3}}\mu, \quad \text{.....(11)}$$

where μ is the average radius of obstacles. In the present discussion, the distances, L and L_p are measured as average values. The angle ϕ_c is a measure of the strength: a weak obstacle can be overcome with a large angle ($\phi_c\sim180^\circ$), whereas strong obstacles can be overcome unless the dislocation practically doubles back on itself ($\phi_c\sim0$). When $\phi_c=0$, the stress $\tau=1.6T/(bL)$ is corresponding to the Orowan stress. The critical angle can be estimated experimentally as follows. The line tension is taken as equal to its energy, that is, $T=Gb^2/2$. When the effective Schmid or Taylor factor (M) is 2.5 for the bcc polycrystalline specimen,[5] the critical angle can be solved uniquely from the yield stress. **Figure 9** shows the change of critical angle as a function of aging time. The angle was found to be large, nearly 180°, indicating that the copper-rich precipitates are very weak obstacles against dislocations.

The interaction force on a dislocation due to an obstacle is expressed by the equation:

$$F=2T\cos(\phi_c/2). \quad \text{.....(12)}$$

Putting the experimentally-determined critical angle into Eq. (12), it is possible to estimate the interaction force. The results are shown in Fig. 9.

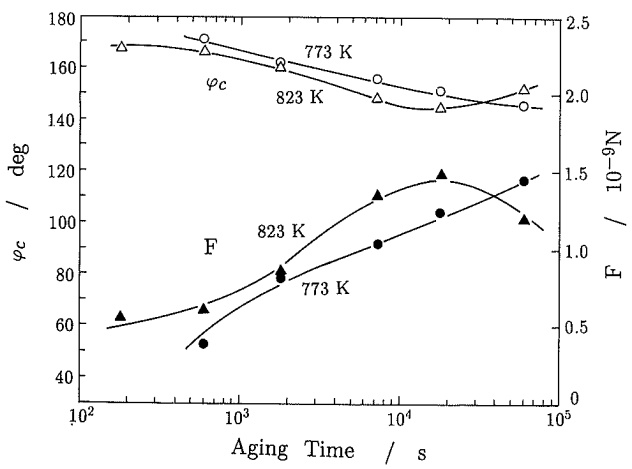

Fig. 9. Aging time dependence of the critical angle (ϕ_c) and the interaction force (F) for Fe–Cu quaternary alloys aged at 773 and 823 K.

4.2. Mechanism for Weak Obstacle

The interaction between cluster and dislocation is typically classified in two regimes[18]: one is the so-called cut-through mechanism, the other is the Orowan mechanism. When clusters are weak obstacles, the former mechanism will preferentially prevail. There are several mechanisms describing the cut-through behavior.

4.2.1. Coherency Strain Effect

When particles with different atomic volume are embedded in the matrix, a strain field is produced around the particle and acts as an internal stress against the movement of dislocation. According to Mott and Nabarro,[19] the internal stress due to the strain field is expressed by the equation,

$$F_{MN}=2Gb|\varepsilon|^{2/3}(bV_f\mu^2)^{1/3}, \quad \text{.....(13)}$$

where ε is the strain. Their theory is applicable to any particles, regardless of their coherency with the matrix. When the $\delta\,(=(r_{Cu}-r_{Fe})/r_{Fe})$ is the misfit of atomic radii, r_{Cu} and r_{Fe}, between Fe and Cu, the strain is given as

$$\varepsilon=\frac{3K\delta}{3K+\dfrac{2E}{1+\nu}}, \quad \text{.....(14)}$$

where K is the bulk modulus of precipitate, and E and ν are the Young modulus and Poisson ratio of the matrix, respectively. Putting experimental data into these physical parameters, ε is estimated to be 1.7% for the Fe–Cu binary system. It should be noted that the Young modulus of copper is about 1/2 of that of iron. **Figure**

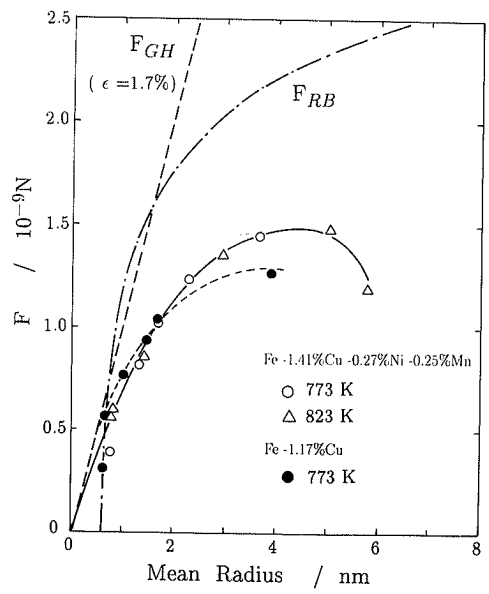

Fig. 10. Particle radius dependence of the interaction force, where F_{GH} and F_{RB} are the theoretical values due to the coherency strain[20] and the elastic modulus effect,[5] respectively.

10 shows the mean radius dependence of the interaction force. When the volume fraction, V_f is 0.012, the force, F_{MN} is estimated to be 0.59×10^{-9} N for the average radius of 2 nm, which is smaller than the experimental values. Therefore, Mott and Nabarro's theory is inadequate to explain the present experimental data.

Gerold and Harberkorn proposed a theory,[20] more precisely concerning the strain field around the coherent particle with the matrix. The force of interaction with dislocation due to a coherent particle with radius μ is expressed by the equation:

$$F_{GH} = 3Gb|\varepsilon_{coh}|\mu\,, \quad \text{.....(15)}$$

where ε_{coh} is the coherency strain. As a first approximation, ε_{coh} is given by Eq. (14). Here, the numerical result of Eq. (15) with $\varepsilon_{coh} = 1.7\%$ is plotted, and is found to be larger than the experimental data. This suggests that the force, F_{GH} can be fitted with the experimental data, when ε_{coh} becomes smaller.

4.2.2. Elastic Modulus Effect

According to Russel and Brown,[5] the interaction between a dislocation and an obstacle of shear modulus lower than the matrix generates an increment of stress for dislocation motion. As this model was based on the difference of shear modulus, it might be called the elastic modulus effect for precipitation hardening. According to their model, the equivalent expression for the force of interaction, F_{RB} is given by the equation:

$$F_{RB} = Gb^2\left[1 - \frac{E_1^2}{E_2^2}\right]^{1/2}, \quad \text{.....(16)}$$

with

$$\frac{E_1}{E_2} = 1 - \frac{E_2^\infty - E_1^\infty}{E_2^\infty}\,\frac{\ln(\mu/r_o)}{\ln(A/r_o)}, \quad \text{.....(17)}$$

where E_1^∞ is the line energy of the dislocation inside the precipitate of infinite volume and E_2^∞ its energy in the matrix; A and r_o are the outer and inner cut-off radii, respectively. The size effect on the force is implicitly included through the change of ratio E_1/E_2. As shown in Fig. 10, F_{RB} is zero at $\mu = r_o = 2.5b$ and increases logarithmically with increasing particle radius.

4.2.3. Chemical Effect

This term is used for the effect occurring from creation of a new interface area during cutting of the dislocation through the particle. The interaction force is given by the equation,

$$F_{CE} = 2\gamma_s b\,, \quad \text{.....(18)}$$

where γ_s is the interfacial energy. It is independent of the particle size. Using the value for the non-coherent interface as $\gamma_s = 0.6\,\mathrm{J/m^2}$ by Goodman *et al.*,[15] F_{CE} is evaluated to be 0.3×10^{-9}, which is very small compared with experimental data as shown in Fig. 10.

4.3. Reconstruction of Yield Stress

Here, we try to explain the yield stress based on the elementary processes of interaction between dislocation and obstacle. As shown in Fig. 10, the interaction force due to the elastic modulus effect increases with increasing mean radius, but it is always larger than the experimental data. It is known that the chemical composition inside precipitates is almost pure copper over the whole range of aging time examined here. In such a case, there is no positive reason to support the continuous change of shear modulus of the precipitate during growth in size as given by Eq. (17). Therefore the elastic modulus effect is suggested to be less effective in the present alloy system.

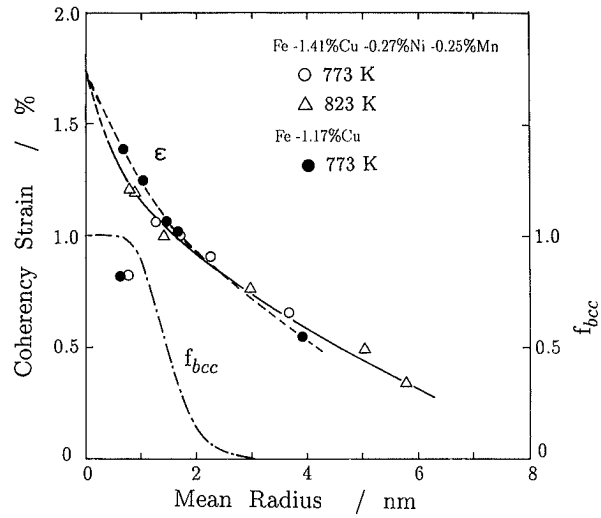

Fig. 11. Particle radius dependence of the coherency strain (ε) together with the fraction of bcc clusters.

As shown in Fig. 10, the interaction force due to coherency strain effect is very large, when the coherency strain was assumed to be 1.7%; this is a theoretically estimated value. By fitting Eq. (15) to experimental data, the coherency strain can be experimentally estimated. **Figure 11** shows the mean radius dependence of the thus-determined coherency strain. The strain decreases with increasing radius. This can be reasonably extrapolated to the theoretical value of 1.7% on the vertical axis. During the phase decomposition, bcc clusters grow in size and transform to fcc phase beyond a critical size. Here, the fraction of bcc clusters (f_{bcc}) in the size distribution is estimated using the equation:

$$f_{bcc} = \frac{N_{p,bcc}}{N_p} = \int_0^{r_c} F(R)dR \Big/ \int_0^{\infty} F(R)dR\,. \quad \text{.....(19)}$$

where $N_{p,bcc}$ and N_p are the number density of bcc and total clusters, respectively. According to the calculation based on the classical nucleation theory,[12] the critical size r_c is reported to be 1.6 nm, where changes of Gibbs energy due to formation of both bcc and fcc clusters become identical. Putting the standard deviation to be 1.35, the fraction is numerically evaluated as a function of mean radius as shown in Fig. 11. The experimentally determined interaction force is an average for numerous precipitates. When obstacles lose coherency by phase transformation, the strengthening effect is reduced. So the apparent interaction force may decrease gradually depending on the decrease of bcc clusters.

All precipitates transform to fcc phase beyond about 3 nm as seen in Fig. 11. According to the coherency strain theory, the strengthening will be reduced. In fact,

however, there remains an elastic strain field around the non-coherent precipitates, even after it is assumed to be at most relaxed by interfacial dislocations. Unfortunately there is at present, no exact theory to treat the strengthening by non-coherent weak obstacles. When this residual strain field around non-coherent precipitates is given by $\varepsilon_{\text{non-coh}}$, the coherency strain effective on the strengthening is proposed to be expressed as

$$\varepsilon = f_{\text{bcc}}\varepsilon_{\text{coh}} + (1 - f_{\text{bcc}})\varepsilon_{\text{non-coh}} \cdot \quad \text{.....(20)}$$

Using this relation, the continuous change of coherency strain in Fig. 11 is well explained. It is particularly suggested that the strengthening due to fcc precipitates is also related to the coherency strain effect through a small residual strain field around non-coherent precipitates.

As shown in the present study, the interaction force due to individual precipitate increases gradually during aging, while the number density of precipitates decreases two orders of magnitude. Therefore, it is concluded that the first increase of yield stress as seen in Fig. 2 is attributable to the growth in size of clusters, but its decrease after the maximum is mainly due to the decrease in number density of precipitates. During this course, the loss of coherency at the interface lowers greatly the strengthening effect. As seen in Figs. 10 and 11, the difference on the interaction force and the coherency strain between the binary and quaternary systems is very small. It is suggested that the segregated layer is elastically similar to the matrix, while the precipitate has a lower Young modulus than the matrix.

5. Conclusion

The behavior of precipitation strengthening in two types of Fe–Cu alloy was investigated by means of mechanical tests as well as SANS measurements. The integrated intensity increased first and reached a constant corresponding to saturation of precipitation reaction, while particle radius increased monotonically with aging time. During aging at temperatures of 773 and 823 K, Vickers hardness and yield stress increased and reached maximum, then decreased. With the aid of structure parameters determined here, the interaction force with a dislocation due to individual precipitate was evaluated and was found to be always less than 30% of Orowan force over the entire aging period. To explain this weak interaction force, four possible mechanisms represented by the keywords of misfit strain, coherency strain, elastic modulus change and interfacial energy have been examined. As a consequence, the strengthening was suggested to be caused from the coherency strain effect. The first increase of yield stress during aging is attributed to the growth in size of clusters and its decrease after the maximum is mainly related to the decrease in number density of precipitates. The loss of coherency with the matrix was suggested to lower greatly the strengthening effect, whereby the structure of precipitates changes from bcc to fcc during aging.

Acknowledgment

The authors wish to express their gratitude to Mr. H. Suzuki of Kawasaki Steel Corp. for the sample preparation. They also thank Drs. R.Uemori and S. Akamatsu, Nippon Steel Corp. for their valuable discussions.

REFERENCES

1) G. Wasserman and P. Wincierz: *Arch. Eisenheuttenw.*, **29** (1958), 310.
2) E. Hornbogen and R. C. Glenn: *Trans. Met. Soc. AIME*, **218** (1960), 1064.
3) E. Hornbogen: *Acta Metall.*, **10** (1962), 525.
4) S. R. Goodman, S. S. Brenner and J. R. Low, Jr.: *Metall. Trans.*, **4** (1973), 2363.
5) K. C.Russel and L. M. Brown: *Acta Metall.*, **20** (1972), 969.
6) J. T. Buswell, C. A. English, M. G. Hetherrington, W. P. Phythian, G. D. Smith and G. M. Worrall: Proc. 14th Int. Symp. on Effects of Radiation in Materials, Andover, Massachussetts, Vol. 2, ASTM-STP 1046, (1988), 127.
7) P. J. Othen, M. L. Jenkins, G. D. Smith and W. J. Phythian: *Phil. Mag. Lett.*, **64** (1991), 383.
8) K. Osamura, H. Okuda, M. Takashima, K. Asano and M. Furusaka: *Materials Trans., JIM*, **34** (1993), 305.
9) E. Hornbogen: *Trans. ASM*, **57** (1964), 120.
10) H. Tamehiro, K. Kishioka, M. Murata, Y. Kawada and A. Takahashi: *Seitetsu Kenkyu*, (1990), No. 337, 34.
11) K. Kishida, O. Akisue, N. Ikenaga, F. Kurosawa and K. Osamura: *J. Jpn. Met. Soc.*, **31** (1992), 538.
12) K. Osamura, H. Okuda, K. Asano, M. Furusaka, K. Kishida, F. Kurosawa and R. Uemori: *ISIJ Int.*, **34** (1994), 346.
13) G. M. Worrel, J. T. Buswell, C. A. English, M. G. Hetherington and G. D. W. Smith: *J. Nuclear Mater.*, **148** (1987) 107.
14) R. Kampmann and R. Wagner: Proc. Conf. on Small Angle Neutron Scattering in Material Science, Springer Verlag, Berlin, (1985), 171.
15) S. R. Goodman, S. S. Brenner and J. R. Low, Jr.: *Metall. Trans.*, **4** (1973), 2371.
16) A. Youle and B. Ralph: *J. Met. Sci.*, **6** (1972), 149.
17) L. M. Brown and R. K. Ham: Strengthening Methods in Crystals, ed. by A.Kelly and R. B. Nicholson, Elsevier, Amsterdam, (1971), 12.
18) P. Haasen: Physikalische Metallkunde, AGNE, (1981), 286.
19) N. F. Mott and F. R. N. Nabarro: Report on Strength of Solids, Phys. Soc., London, (1948).
20) V. Gerold and H. Harberkorn: *Phys. Stat. Sol.*, **16** (1966), 675.